# Improving the Response of Optical Phase Modulators in SOI by Computer Simulation

P. D. Hewitt and G. T. Reed

***Abstract*—This paper reports on the simulation of a low-loss single-mode optical phase modulator fabricated in silicon-on-insulator (SOI) material. The device operates by injecting free carriers to change the refractive index in the guiding region, and has been modeled using the two-dimensional (2-D) device simulation package SILVACO. SILVACO has been employed to optimize the overlap between the injected free carriers in the intrinsic region and the propagating optical mode. Attention has been paid to both the steady state and transient properties of the device. In order to produce quantitative results, a particular p-i-n device geometry has been employed in the optimization, but the trends in the results are general enough to be of help in the design of many modulator geometries. The specific example device we have used is designed to support a single optical guided mode and is of multimicrometer dimensions thus simplifying fabrication and allowing efficient coupling to–from single-mode fibers (SMF's) or other single-mode devices. The modeling indicates that increased dc device performance results from an increase in the doping concentrations and the contact diffusions of the $p^+$ and $n^+$ regions. The transient performance of the device in terms of switching times depends on the separation of the $p^+$ and $n^+$ regions. The optimizations are applicable to large (multimicrometer size) modulators. Phase modulators with low driving currents (<8 mA) and modulators with transient rise times of 39 ns and fall times of 6 ns are predicted.**

***Index Terms*—Carrier injection, phase modulation, rib waveguides, silicon-on-insulator (SOI).**

## I. Introduction

OPTICAL switches and modulators are essential components for some integrated optics applications. In this paper, we analyze a particular geometry of an optical phase modulator in silicon-on-insulator (SOI) material using the two-dimensional (2-D) semiconductor simulation package SILVACO. While the results are specific to the chosen device geometry, some of the results are general enough to enable improvement of the performance of many other device geometries.

In recent years, silicon integrated optics has become interesting for a range of applications, due in part to moderate performance at low cost (e.g., [1]–[8], [10]–[13]). Silicon exhibits losses <0.1 dB/cm [1] in the infrared (1.3–1.5 $\mu$m) and hence the potential exists for the fabrication of active and passive silicon devices at these wavelengths. The first optical waveguides in silicon were proposed and fabricated by Soref and Bennett in 1986 [1], whose devices were epitaxially grown doped silicon-on-silicon, although it is now widely accepted that SOI structures are more versatile. This is because the SOI structure is strongly confining and low loss. A rib structure leads to vertical confinement of the optical mode as a result of the high refractive index difference between the air/silicon/$SiO_2$ and horizontal confinement results from the etched rib, enabling bends and interconnections to be produced much more easily than in structures which confine the optical mode less well. Losses as low as 0.3 dB/cm have been demonstrated for SOI waveguides [2].

Manuscript received March 31, 1999; revised November 19, 1999. This work was supported by Bookham Technology Ltd. The work of P. D. Hewitt was supported by EPSRC.

The authors are with the School of Electronic Engineering, Information Technology and Mathematics, University of Surrey, Guildford, Surrey GU2 5XH, U.K.

Publisher Item Identifier S 0733-8724(00)02188-5.

## II. Modulation Mechanisms

### A. The Free Carrier Dispersion Effect

Unstrained pure crystalline silicon exhibits no linear electrooptic (Pockels) effect. Soref and Bennett experimentally studied the refractive index changes in silicon due to the Franz–Keldysh effect, Kerr effect, and charge carrier effects [3]. They found that the Franz–Keldysh effect and the Kerr effect were very weak in silicon. For the Kerr effect, an applied field in the range $10^4$ to $3 \times 10^5$ V/cm produces a change in refractive index ($n$) of the order of $10^{-8}$ to $10^{-5}$ [3]. Therefore, high fields potentially close to the breakdown of silicon are required to obtain a useful refractive index change. They also showed that the most effective mechanism for varying the refractive index/optical absorption of light in pure silicon is the free carrier plasma dispersion effect, which also has an added advantage of being polarization independent.

A study of the free carrier effect was carried out by Soref *et al.* [4], who obtained the changes in refractive index and absorption coefficients at both wavelengths of interest ($\lambda = 1.3$ and $\lambda = 1.55$ $\mu$m) as a function of free electron and free hole concentration.

For $\lambda = 1.3$ $\mu$m

$$\Delta n = \Delta n_e + \Delta n_h = -[6.2 \times 10^{-22}.\Delta N_e + 6.0 \times 10^{-18}.(\Delta N_h)^{0.8}] \quad (1)$$

$$\Delta\alpha = \Delta\alpha_e + \Delta\alpha_h = 6.0 \times 10^{-18}.\Delta N_e + 4.0 \times 10^{-18}.\Delta N_h. \quad (2)$$

For $\lambda = 1.55$ $\mu$m

$$\Delta n = \Delta n_e + \Delta n_h = -[8.8 \times 10^{-22}.\Delta N_e + 8.5 \times 10^{-18}.(\Delta N_h)^{0.8}] \quad (3)$$

and

$$\Delta\alpha = \Delta\alpha_e + \Delta\alpha_h = 8.5\times10^{-18}\Delta N_e + 6.0\times10^{-18}\Delta N_h \quad (4)$$

where

- $\lambda$ free space wavelength;
- $\Delta n_e$ change in refractive index resulting from change in free electron carrier concentrations;
- $\Delta n_h$ change in refractive index resulting from change in free hole carrier concentrations;
- $\Delta\alpha_e$ change in absorption coefficient resulting from change in free electron carrier concentrations;
- $\Delta\alpha_h$ change in absorption coefficient resulting from change in free hole carrier concentrations.

From (1) and (3), it is noted that the change in refractive index decreases as the number of injected carriers increases, and that the change in refractive index is greater for a given number of injected carriers at the longer wavelength of $\lambda = 1.55$ $\mu$m. It can also be noted from (2) and (4) that a finite change in the silicon refractive index must also result in a finite change in the absorption. A change in the refractive index/absorption in silicon due to the plasma dispersion effect, can be achieved by means of carrier injection or depletion of both electrons and holes into the intrinsic region of a forward biased silicon p-i-n diode. Soref and Bennett [3] confirmed that for experimentally reasonable values of applied field and injected carriers, the changes in refractive index were at least two orders of magnitude larger for the free carrier plasma effect than for the other electric field effects mentioned above.

### B. Thermooptic Effect

The thermooptic effect is a change in the refractive index of silicon due to a change in the temperature of the silicon. As the temperature changes, the energy bandgap, and hence the refractive index vary. For $\lambda = 1.5$ $\mu$m the thermal change of the refractive index of silicon is given by [5]

$$\delta n/\delta T = +1.86\times10^{-4}K^{-1}. \quad (5)$$

The thermooptic effect is rather slow, and hence to date thermooptic devices have been fabricated with modulation applications typically up to 1 megahertz [6]. One example is the device reported by Cocurollo *et al.* [6] which had a 3-dB bandwidth of 700 kHz. Therefore all applications requiring higher modulation frequencies of the megahertz range and above, are usually based on the free carrier plasma dispersion effect. In contrast to the free carrier injection which reduces the refractive index of silicon, the thermooptic effect increases the refractive index of silicon. Our device will be shown to operate in the megahertz range (i.e., rise/fall times <500 ns), thus reducing thermal effects. It has also been shown that for similar p-i-n devices the thermooptic effect can be neglected [7], [12], [13].

## III. Device Structure

### A. Geometry

The device structure to be considered in this paper is of a lateral optical phase modulator integrated into a low loss SOI rib waveguide. The cross section of the active region of the device is shown in Fig. 1, and represents the geometry used in all simulations unless otherwise stated. All the dimensions and doping characteristics described below are used throughout this report unless otherwise stated. This device will be referred to as the reference modulator, such that any variations in device geometry or doping profiles/concentrations are implicitly to be compared to the reference modulator in order to demonstrate an improvement or degradation in device performance. The interaction length is defined as the active length of the device in the $z$-direction. We have assumed that all the devices are electrically and optically homogeneous in the $z$-direction.

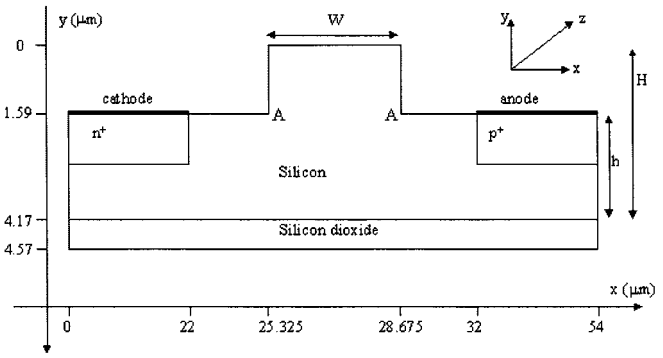


Fig. 1. The geometry of the device which is referred to as the reference modulator.

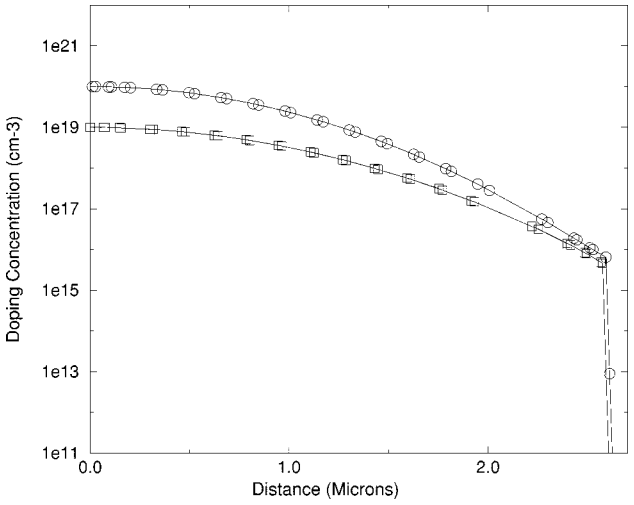


Fig. 2. Doping profiles of the $n^+$ (—O—) and $p^+$ (— —) regions of the reference device.

Fig. 2 shows a cross section of the doping profiles in the $y$-direction for the reference device of Fig. 1, used in the simulations. The cross section through the $n^+$ doped region is from $y = 1.59$ to $y = 4.57$ $\mu$m with $x = 10$ $\mu$m. The cross section through the $p^+$ doped region is from $y = 1.59$ to $y = 4.57$ $\mu$m with $x = 42$ $\mu$m. The $p^+$ and $n^+$ doped regions shown in Fig. 2 are of a Gaussian profile.

## IV. Electrical and Optical Analysis

The two-dimensional simulation package SILVACO [9] has been employed to investigate the dc and transient behavior of the modulator. SILVACO is a physically based simulator which predicts the electrical characteristics associated with specified

physical structures and conditions. This is achieved by solving partial differential equations which describe semiconductor physics such as Poisson's equation and the charge continuity equations for electrons and holes. Physical-based simulators are predictive and provide insight into the internal physical mechanisms associated with device operation. Often these internal physical mechanism are very difficult or impossible to measure experimentally. For our purpose, SILVACO has been used to predict the injected free carrier densities in the intrinsic region of the device for a range of different device geometries and working conditions. This approach has been validated in the past by experimental verification of predicted device performance [7]–[10]. A change in refractive index of the silicon guiding layer will result from an injection of free carriers into the guiding region. In order to maximize the change in refractive index we must optimize the interaction between the injected free carriers and the propagating optical guided mode. The rib is single mode as it satisfies the condition for single mode operation [8].

Although SILVACO does not calculate the overlap integral between electrical carriers and optical field, it will be demonstrated that there is a high degree of uniformity of the predicted injected carrier concentration at the levels of interest, throughout the central guiding region of the structure. This will clearly result in a relatively uniform refractive index change across the waveguiding region. We can therefore obtain from SILVACO the mean value of the injected carrier concentration in the guiding region, and apply the result to (3) and (4) to obtain the resulting change in refractive index and absorption for the device under investigation at a wavelength of $\lambda = 1.55$ $\mu$m. The change in refractive index results in a phase shift $\Delta\phi$ in the optical mode given by

$$\Delta\phi = 2\pi\Delta n L/\lambda \tag{6}$$

where $L$ = active length of the modulator in the $z$-direction.

We can also estimate the length $L_\pi$ required to produce a phase shift for our device from

$$L_\pi = \lambda/(2\Delta n). \tag{7}$$

## V. Simulation Results

### A. Reference Modulator

*1) Modeling Characteristics:* The device was modeled assuming ohmic contacts with no additional contact resistance or capacitance. The Shockley–Reed–Hall recombination carrier lifetime in the intrinsic region are $\tau_n = 700$ ns, $\tau_p = 300$ ns, where $\tau_n$ = electron lifetime and $\tau_p$ = hole lifetime. The values of $\tau_n$ and $\tau_p$ were chosen as they correspond to a realistic intrinsic epilayer doping layer of $10^{15}$ cm$^{-3}$ [13]. It is expected that a device with shorter intrinsic carrier lifetimes than that stated above will have superior switching capabilities but at the expense of greater power requirements, and similarly a device with longer intrinsic carrier lifetimes will have lower power consumption but poorer switching capabilities. One method of reducing the carrier lifetime of the intrinsic region is to include a lifetime killer such as gold.

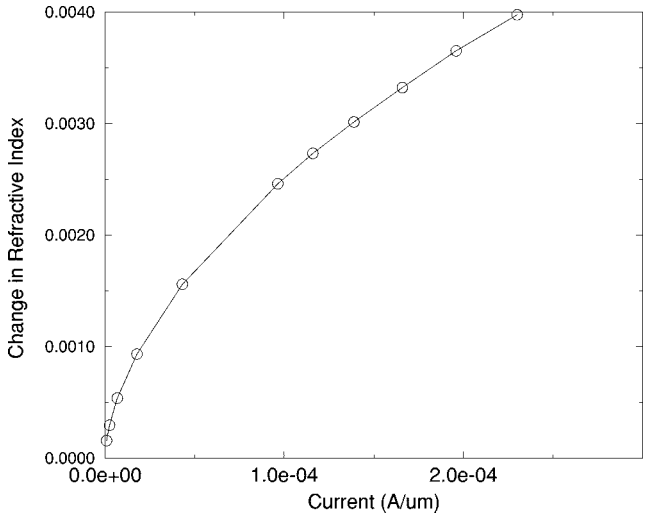


Fig. 3. Change in refractive index versus current for the reference modulator of Fig. 1.

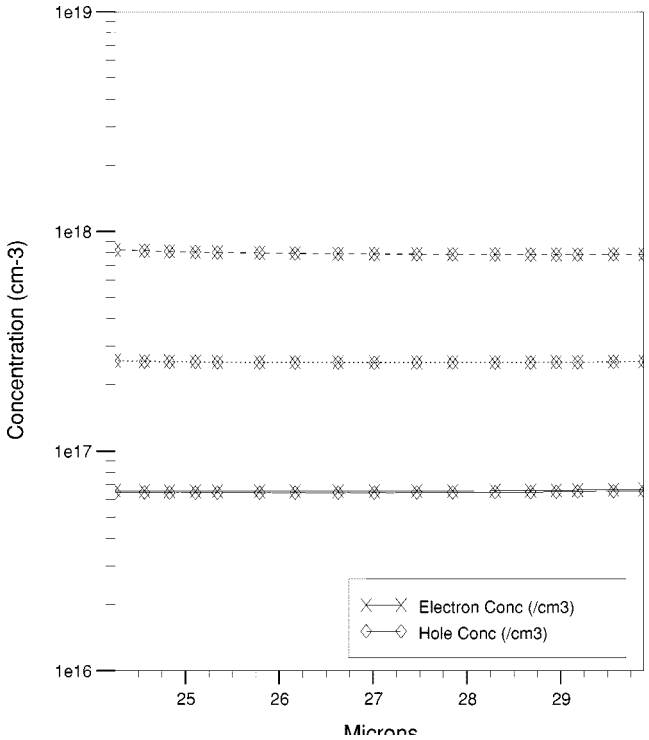


Fig. 4. Injected free carriers along a vertical section ($y = 2$) through the optical channel for the reference modulator. Applied voltage $(V) = 1.00$ V for the top plot, 0.92 V for the middle plot and 0.84 V for the bottom plot.

*2) Phase Modulation and Absorption:* Fig. 3 shows the dc change in refractive index against current for the device of Fig. 1. The optical wavelength is $\lambda = 1.55$ $\mu$m. Fig. 3 shows that the change in refractive index varies nonlinearly with applied current. One factor, which contributes to the nonlinearity of the change in refractive index versus current density relation, is the sublinear dependence of the change in free holes $N_h$ with the change in refractive index, as shown in (1) and (3). Also, as we drive the modulator harder, we inject more free carriers into the intrinsic region of the device. The increase in the concentration of the intrinsic region results in an increase in the Auger recombination rate (at injected carriers concentrations much greater

TABLE I
RISE AND FALL TIMES FOR THE REFERENCE MODULATOR AND THE ROUNDED WALL MODULATOR OF FIG. 7, WITH VARIOUS VALUES OF $R$

| Modulator | Rise time $t_r$ (ns) | Fall time $t_s$ (ns) |
|---|---|---|
| Reference | 95 | 22 |
| Rounded wall : R=0.5μm | 101 | 22 |
| Rounded wall : R=1.0μm | 106 | 22 |

than $10^{17}$ cm$^{-3}$ the Auger recombination becomes the dominant recombination process). This results in a reduced lifetime in the intrinsic region and hence we have to drive the modulator harder to achieve an equivalent refractive index change than at lower drive powers. Of course an increase in the recombination of the intrinsic device will result in a faster switching device, i.e., reduction in the rise and falls times of the modulator.

*3) Switching Characteristics:* The switching characteristics of the device illustrated in Fig. 1 were evaluated using a transient solution. This involved initially applying a reversed biased voltage of $-5$ V to the p-i-n structure for a time of 20 ns. The reverse bias results in the depletion of free carriers from the intrinsic region. A forward bias step was then applied to the device for 300 ns, with a 1 ns rise time and a 1 ns fall time. During the fall section of the step bias the voltage is stepped down to the initial reverse bias voltage of $-5$ V. The value of applied voltage to the anode for the forward bias step was chosen so that the steady state induced phase modulation at that voltage was approximately $\pi$ radians. The interaction length of the device is 500 $\mu$m.

The rise time $t_r$ is defined, as the time required for the induced phase shift to change from 10% to 90% of the maximum value. Likewise, the fall time $t_f$ is defined as the time required for the induced phase shift to change from 90% to 10% of the maximum value. The switching characteristics were calculated for the reference device with an interaction length of 500 $\mu$m. The rise and fall times determined are $t_r = 95$ and $t_f = 22$ ns, respectively.

*4) Injected Free Carriers in the Intrinsic Region:* Fig. 4 shows predictions of the injected electron and hole concentrations along a horizontal section through the center of the waveguiding region for the reference device with an interaction length of 500 $\mu$m. The injected plasma shows good uniformity in the intrinsic region for the applied forward biases of interest. The maximum variation in the concentration of the injected carriers through the center of the waveguiding region is seen to be less than 2%. Analogous plots along the vertical direction yield the same sense of uniformity of injected carriers. We can therefore justifiably make the assumption of a constant profile of injected carriers in the intrinsic region for the range of voltage biases of interest. This assumption simplifies the resulting calculations of change in refractive index and change in absorption for the modulator.

### *B. Device Characteristics for the Modulator with Rounded Edges*

This section considers the effect of rounded edges at the base of the rib, which may occur during fabrication of a real device. The curvature occurs at points $A$, illustrated in Fig. 1 with radius of curvature, $R$. The interaction length of the modulator is 500 $\mu$m. All other device dimensions and the device doping profiles are identical to those of the reference modulator.

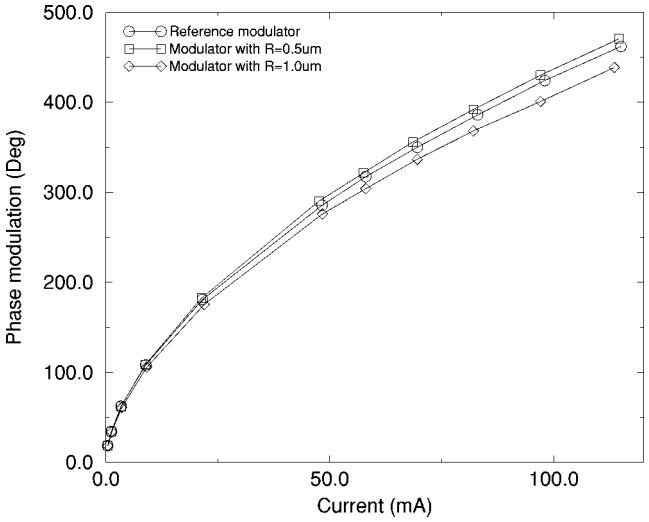


Fig. 5. Phase modulation against current for the reference modulator and the rounded wall device illustrated in Fig. 8.

The results illustrated in Fig. 5 indicate that there is an optimum value of $R$ for the rounded wall device, which will result in a small improvement in device performance in terms of phase modulation against current. The improvement is in comparison with the straight right-angled rib walled reference modulator. The improvement appears to be greatest for a radius of curvature $R = 0.5$ $\mu$m. For example, the reference modulator requires a current of 73 mA to achieve a $2\pi$ phase shift, whereas for the rounded wall modulator with $R = 0.5$ $\mu$m, a forward current of 70 mA is required to achieve a 2-$\pi$ phase shift, an improvement of approximately 4%. Intuitively less crowding of carriers would be expected at a curved corner than at an abrupt corner. This suggests that perhaps more carriers will occupy areas of the waveguide in which the optical mode propagates, although this is likely to be a small effect. The results of the modeling confirm this.

Table I compares the rise and fall times for the reference modulator and two modulators with rounded walls, obtained from a transient solution Fig. 6. For the three modulators investigated, the transient solution produced rise and fall times that were very similar. For the modulators studied above, there is a small increase in the rise time with an increase in the radius of curvature, whereas the fall times are constant. Overall, the results indicate that the modulator performance in terms of dc and transient performance is not significantly influenced by the small change from a straight rib wall to one which has a small radius of curvature, at the base of the rib.

TABLE II
CURRENT REQUIRED TO PRODUCE A $\pi$ PHASE SHIFT AND THE RISE/FALL TIMES FOR THE REFERENCE MODULATOR WITH VARIOUS DOPING PROFILES AND CONCENTRATIONS

| Doping profile | n+ doping conc. ($cm^{-3}$) | depth ($\mu$m) | p+ doping conc. ($cm^{-3}$) | depth ($\mu$m) | $I_\pi$ (mA) | rise time (ns) | fall time (ns) |
|---|---|---|---|---|---|---|---|
| | | | | | | | |
| Constant | $1x10^{20}$ | 2.5 | $1x10^{19}$ | 2.5 | 8 | 105 | 25 |
| Constant | $1x10^{20}$ | 1.4 | $1x10^{19}$ | 1.7 | 18 | 164 | 30 |
| Gaussian (reference device) | $1x10^{20}$(peak) | | $1x10^{19}$(peak) | | 21 | 95 | 22 |
| Gaussian | $1x10^{19}$(peak) | | $1x10^{18}$(peak) | | 63 | 110 | 25 |
| Gaussian | $1x10^{18}$(peak) | | $1x10^{17}$(peak) | | >150 | | |

where $I_\pi$ = Current required to produce a $\pi$ phase shift

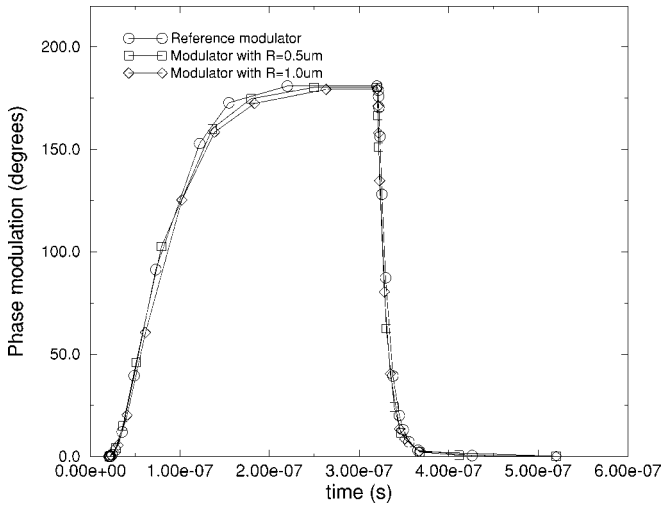


Fig. 6. Phase modulation against time, when a square wave input of 300-ns long is applied to the reference modulator and the rounded wall device.

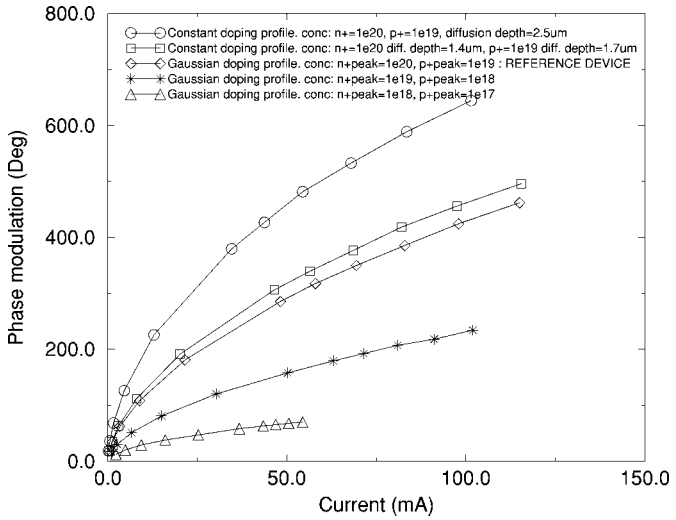


Fig. 7. Phase modulation versus current for various doping profiles and concentrations.

## C. Doping Effects

The effects on the device performance due to changes in doping concentrations, doping diffusion depths and doping profiles of the $p^+$ and $n^+$ regions has been investigated. The two types of doping profiles considered were a constant profile and a Gaussian profile.

For the constant concentration profile, a study of the depth of the profile on the modulator performance was made. For the modulators with Gaussian concentration profiles, a study of the change in the concentration levels of the Gaussian profiles on the modulator performance was made. A comparison was also made regarding the significance of the type of doping profile to the modulator performance. The results are shown in Table II, and Figs. 7 and 8. The interaction length of the active region of the device is 500 $\mu$m.

*1) Effect of Diffusion Depth:* The depth of the contact diffusion does affect the performance of the modulator. The first modulator studied had a 2.5-$\mu$m vertical diffusion depth measured from the contact. The depth was the same for both the $p^+$ and the $n^+$ doped regions. The second modulator had an $n^+$ diffusion depth of 1.4 $\mu$m and a $p^+$ diffusion depth of 1.7 $\mu$m. For the modulator with the deeper diffusion depth a forward current of 8 mA was required to achieve a $\pi$ phase shift, whereas for the modulator with the shallower diffusion depth a forward current of 18 mA was required to achieve a $\pi$ phase shift. Hence, in this example a factor two reduction occurred in the drive current, simply by increasing the diffusion depth of the $p^+$ and the $n^+$ doped regions.

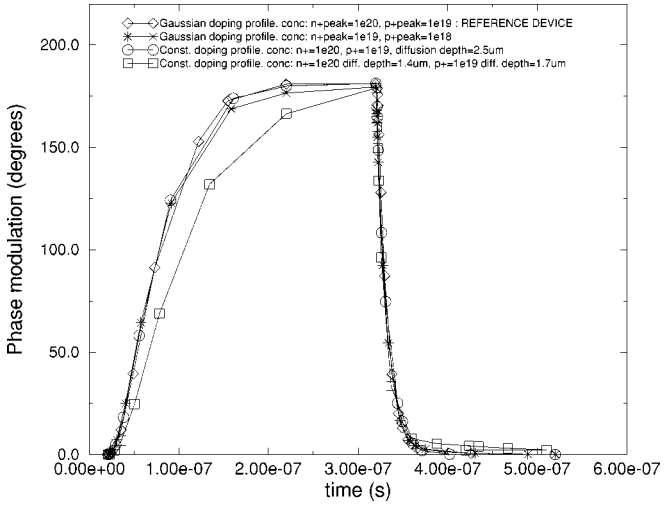


Fig. 8. Phase modulation versus time for various doping profiles and concentrations, when a square wave input of 300 ns long is applied.

The transient response also yielded improvements in the rise and fall times for the modulators with increased diffusion depths. The rise and fall times were 164 and 30 ns, respectively, for the modulator with the shallower diffusion depth, whereas the rise and fall times for the modulator with the deep diffusion depth had decreased to 105 and 25 ns, respectively.

The increase in both the dc and transient performance with increasing diffusion depth is partly due to the increase in the number of free electrons and holes, which are available for injection in to the guiding region. Additionally, increasing the diffusion depth increases the area of the injecting contact adjacent to the waveguiding region. A shallow diffusion depth tends to result in a larger proportion of the injected carries residing in the region directly below the doping regions, where a smaller proportion of optical mode exists. An increase in the diffusion depth of the $p^+$ and $n^+$ doped regions results in improved injection efficiency of free carriers into the regions where the majority of the optical mode propagates.

The above calculations were made for constant concentration profiles. Clearly, in a real diffusion the concentration profiles will vary, but the conclusions reached regarding the depth of diffusion will still be applicable. The disadvantage in a deep diffusion is an increase the complexity of the fabrication process, although the deep doping level could be achieved by other means such as ion implantation.

*2) Effect of Doping Concentration:* The concentration of the doping regions also affects the dc and transient performance of the modulator. For a range of Gaussian doping concentration profiles as shown in Figs. 7 and 8 and Table II, the results indicate that an increase in the modulator's dc and transient performance is superior for high doping concentrations.

For example, the reference device has a peak doping concentration of $1 \times 10^{20}$ cm$^{-3}$ in the $n^+$ region and a peak doping concentration of $1 \times 10^{19}$ cm$^{-3}$ in the p region. To achieve a $\pi$ phase shift for a modulator of 500-$\mu$m interaction length, a forward current of 21 mA is required. For a similar device with a peak doping concentration of $1 \times 10^{19}$ cm$^{-3}$ in the $n^+$ region and a peak doping concentration of $1 \times 10^{18}$ cm$^{-3}$ in the $p^+$ region, to achieve a $\pi$ phase shift for a modulator of 500-$\mu$m interaction length a forward current of 63 mA is required. Consequently, there is a reduction in the current required for a $\pi$ phase shift by a factor of three, for the modulator with higher peak doping concentration.

Increasing the doping concentrations of the $p^+$ and $n^+$ regions also results in a decrease in $t_r$ and $t_f$. For the two devices compared above, $t_r$ was 110 ns for the lower doping and 95 ns for the higher and similarly $t_f$ was 25 and 22 ns, respectively.

An increase in the doping concentration of the $p^+$ and $n^+$ regions will increase the absorption of the optical mode that propagates through the $p^+$ and $n^+$ regions. Also the increase in the doping concentration of the $p^+$ and $n^+$ regions will result in an increase in the refractive index difference between the intrinsic region and the $p^+$ and $n^+$ regions, resulting in a stronger confinement of the propagating optical mode in the intrinsic region, therefore a smaller portion of the optical mode will propagate in the highly doped $p^+$ and $n^+$ regions. We can make an approximation of the absorption during dynamic operation using (4). Assuming that the optical mode is strongly confined in the intrinsic region and the number of injected carriers in this region is $5 \times 10^{17}$ cm$^{-3}$, from (4) the absorption $\alpha = 7.25$ cm$^{-1}$ (i.e., $\sim$31.5 dB/cm). If the active length of the device is 500 $\mu$m then the additional optical absorption is approximately 1.6 dB.

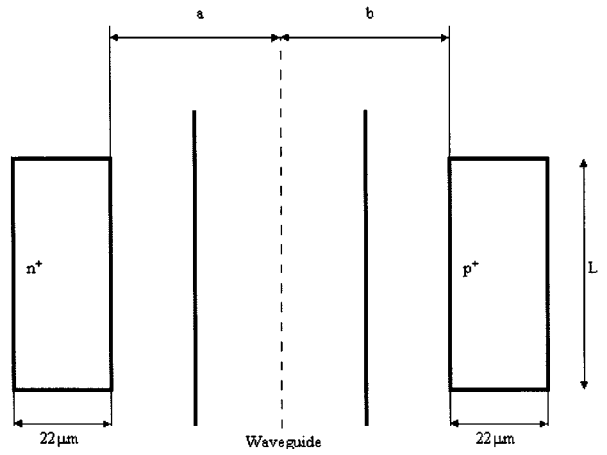


Fig. 9. Location of the doping window.

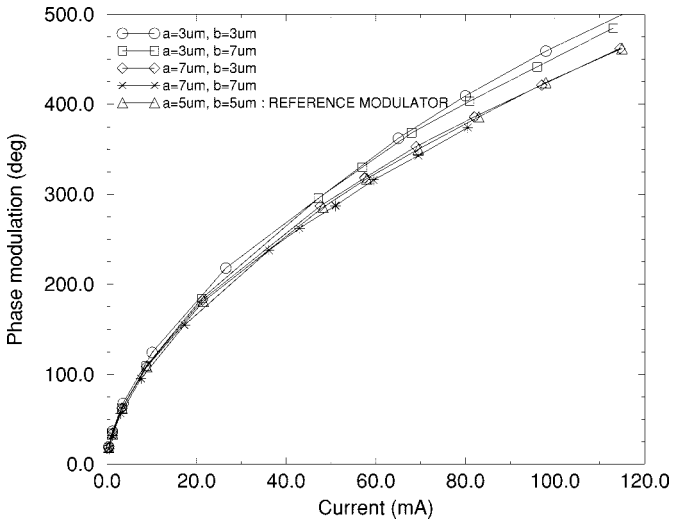


Fig. 10. Phase modulation against current for changes in the location of the doping windows.

### D. The Effects Due to the Position of the Doping Windows

An evaluation of the modulator performance was made in terms of the displacement of the doping windows from the center of the waveguide. A plan view of the geometry of the modulator is illustrated in Fig. 9. The variables $a$ and $b$ were investigated in terms of the device performance. The interaction length of the modulator is 500 $\mu$m.

*1) DC Characteristics:* The results indicate (Fig. 10) that there is increased performance in terms of induced phase modulation against current if the doping windows are placed close to the center of the waveguide. This is a consequence of the reduction in the cross-sectional area of the intrinsic region between the $p^+$ and $n^+$ regions. Also with decreasing separation of the $p^+$ and $n^+$ doped regions, the confined region where the majority of the optical mode propagates is also reduced.

A disadvantage is that this may result in an increase in the absorption of the device. If we consider that the $p^+$ and $n^+$ re-

TABLE III
RISE AND FALL TIMES FOR THE DEVICE OF FIG. 1 WHEN A SQUARE WAVE INPUT SIGNAL 300 ns IS APPLIED

| Separation of windows a(μm) | Separation of windows b(μm) | Rise time $t_r$(ns) | Fall time $t_f$(ns) |
|---|---|---|---|
| 3 | 3 | 39 | 6 |
| 3 | 7 | 104 | 32 |
| 5 | 5 | 95 | 22 |
| 7 | 3 | 92 | 14 |
| 7 | 7 | 184 | 50 |

gions are heavily doped, the optical mode confinement will be well-enhanced laterally and hence absorption due to the tail of the optical mode extending into the $p^+$ and $n^+$ regions will be reduced, although conversely the tail of the mode extending into the doped region will suffer increased absorption.

For the two extreme positions of the doping windows investigated, the forward current required to produce a $\pi$ phase shift for the modulator with $a = 7$ and $b = 7$ $\mu$m (see Fig. 9) is 23 mA, whereas the forward current required to produce a $\pi$ phase shift for the modulator with $a = 3$ and $b = 3$ $\mu$m is 20 mA. Therefore, increasing the spacing of the doping regions from $a = b = 3$ to $a = b = 7$ $\mu$m results in an increased current of 15%.

One interesting result is that the modulator with doping windows at $a = 3$ and $b = 7$ $\mu$m slightly out performs the modulator with doping windows at $a = 7$ and $b = 3$ $\mu$m, in terms of phase modulation against forward current. This may be due to the higher concentration $n^+$ region being closer to the center of the rib in the former case.

*2) Switching Characteristics:* Fig. 11 illustrates the phase modulation against time for the modulator with varying values of $a$ and $b$, when a square wave input signal of duration 300 ns is applied. The results indicate that the distance of the doping regions from the center of the rib affects the switching characteristics of the modulator more than any other effect studied in this paper. An improvement of greater than four times in the rise and fall times of the transient response results from decreasing the separation of the windows from $a = b = 7$ to $a = b = 3$ $\mu$m. The switching times are summarized in Table III.

Clearly there is an associated improvement in the lateral confinement of the optical mode when the $p^+$ and $n^+$ regions are translated toward the center of the rib. Hence this results in reduced switching times due to the reduction in the time taken to fill or deplete the area where the optical mode now propagates. Also, the modulator with $n^+$ and $p^+$ regions closer to the center of the rib results in an increased refractive index change for a given current density, than a modulator with $p^+$ and $n^+$ regions further from the center of the rib. Hence, moving the $n^+$ and $p^+$ regions closer to the center of the rib results in increased dc and transient modulator performance.

SILVACO automatically calculates the capacitance of the device, which varies with applied voltage. At a forward bias of 1.0 V the capacitance is approximately $1\times10^{-12}$ $F/\mu$m, which corresponds to a device capacitance of 500 pF. Assuming we connect the device to a 50-$\Omega$ source, the rise time will be similar to those quoted in table confirming the basis of our argument.

Interestingly the modulator with $n^+$ and $p^+$ regions at $a = 3$ and $b = 7$ $\mu$m slightly under performs the modulator with

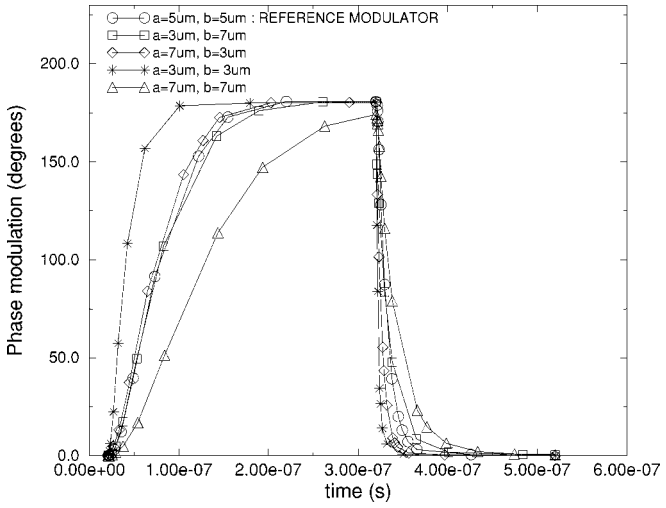


Fig. 11. Phase modulation versus time for changes in the location of the doping windows when a square wave input signal 300 ns is applied.

$n^+$ and $p^+$ regions at $a = 7$ and $b = 3$ $\mu$m in terms of rise and fall times. This is likely to be due to the slightly increased recombination rate in the intrinsic region for the modulator with $n^+$ and $p^+$ regions at $a = 7$ and $b = 3$ $\mu$m, or due to the different injection efficiencies of the $n^+$ and $p^+$ regions.

## VI. CONCLUSION

The free carrier plasma effect offers a means for electrically controlled optical modulation in a silicon waveguide. It has been shown that effective and efficient phase modulation can be achieved in silicon by use of a p-i-n diode structure to inject charge carries into an SOI waveguide.

We have analyzed the performance of a p-i-n diode integrated into an SOI rib waveguide. The SOI rib waveguide is of multimicrometer dimensions, thus allowing efficient coupling to optical fibers. A 2-D semiconductor simulation package SILVACO was employed to investigate the dc and transient behavior of the active region of the modulator, via the solution of the Poisson and continuity equations. It was demonstrated that a high degree of uniformity of the injected carrier concentrations is predicted in the guided region of the modulator, thus simplifying the optical mode analyses.

We have studied the effects of rounded rib edges, doping profiles, doping concentration, diffusion depths, and alignment of the doped regions, on both the static and dynamic behavior of the phase modulator. The results indicate that the modulator dc performance depends mostly on the doping profile, concentration and diffusion depth of the $p^+$ and $n^+$ doped regions,

whereas the dynamic behavior is influenced mainly by the lateral positions of both the $p^+$ and $n^+$ doped regions.

The predictive results indicate the potential for the fabrication of devices with interaction lengths of 500 $\mu$m with drive currents as low as $<8$ mA for a phase modulation of $\pi$ radians. Furthermore by decreasing the separation of the $p^+$ and $n^+$ region from the center of the rib waveguide an improvement in the switching characteristics of the modulator occurs. The predicted results indicate that switching rise time can be reduced to 39 ns and fall time to 6 ns.

These predicted results are very promising and indicate scope for further optimization of experimental devices. While this paper discusses the results of a specific phase modulator design, the results suggest that deep diffusions and close lateral separation of the diffusions would also enhance the performance of other p-i-n phase modulator geometries, although there would clearly need to be a specific evaluation of any given design.

## ACKNOWLEDGMENT

The authors would like to thank SILVACO International for the device modeling software.

## REFERENCES

[1] R. A. Soref and J. P. Lorenzo, "All silicon active and passive guided-wave components for $\lambda = 1.3\mu$m and $1.6\mu$m," *IEEE J. Quantum Electron.*, vol. QE-22, pp. 873–879, 1986.

[2] A. Rickman, G. T. Reed, B. L. Weiss, and F. Namavar, "Low loss planar optical waveguides fabricated in SIMOX material," *IEEE Photon. Technol. Lett.*, vol. 4, pp. 633–635, 1992.

[3] R. A. Soref and B. R. Bennett, "Electrooptical effects in silicon," *IEEE J. Quantum Electron.*, vol. QE-23, pp. 123–129, 1987.

[4] ——, "Kramers-Kronig analysis of E-O switching in silicon," *SPIE Integr. Opt. Circuit Eng.*, vol. 704, 1986.

[5] G. Cocorullo and I. Rendina, "Thermooptical modulation at 1.5 $\mu$m in silicon etalon," *SPIE Integr. Opt. Circuit Eng.*, vol. 704, 1986.

[6] C. Cocorullo, M. Iodice, I. Rendina, and P. M. Sarro, "Silicon thermooptical micro-modulator with 700 kHz-3 dB bandwidth," *IEEE Photon. Technol. Lett.*, vol. 7, pp. 363–365, 1995.

[7] C. K. Tang and G. T. Reed, "Highly efficient optical phase modulator in SOI waveguides," *Electron. Lett.*, vol. 31, no. 6, pp. 451–452, 1995.

[8] R. A. Soref, J. Schmidtchen, and K. Petermann, "Large single-mode rib waveguides in GeSi and Si-on-SiO2," *J. Lightwave Technol.*, vol. 9, pp. 1971–1974, 1991.

[9] SILVACO International, 4701 Patrick Henry Drive, Bldg. 1, Santa Clara, CA 94054.

[10] C. K. Tang, G.T. Reed, A. J. Walton, and A. G. Rickman, "Low loss, single-mode, optical phase modulator in SIMOX material," *J. Lightwave Technol.*, vol. 12, pp. 1394–1400, Aug. 1994.

[11] T. D. Bestwick, "Active silicon integrated optical circuits," in *Proc. Mater. Res. Soc. Symp.*, vol. 486, 1998, pp. 57–65.

[12] G. Breglio, A. Cutolo, M. Iodice, P. Spirito, and L. Zeni, "Simulation and analysis of silicon electro-optic modulator utilizing a three terminal active device and integrated in a silicon-on-insulator low loss single mode waveguide," in *Proc. SPIE—Int. Soc. Opt. Eng.*, vol. 3007, USA, 1997, pp. 40–47.

[13] A. Cutolo, M. Iodice, P. Spirito, and L. Zeni, "Silicon electro-optic modulator based on a three terminal device integrated in a low-loss single-mode SOI waveguide," *J. Lightwave Technol.*, vol. 15, pp. 505–518, Mar. 1997.

**P. D. Hewitt**, photograph and biography not available at the time of publication.

**G. T. Reed**, photograph and biography not available at the time of publication.